Spectrochimica Acta Part A: Molecular and Biomolecular Spectroscopy 118 (2014) 42–47

Contents lists available at ScienceDirect

Spectrochimica Acta Part A: Molecular and Biomolecular Spectroscopy

journal homepage: www.elsevier.com/locate/saa

Raman investigations of Upper Cretaceous phosphorite and black shale from Safaga District, Red Sea, Egypt

Valerian Ciobotă [a], Walid Salama [b,c], Paul Vargas Jentzsch [a], Nicolae Tarcea [a], Petra Rösch [a], Ahmed El Kammar [c], Rania S. Morsy [c], Jürgen Popp [a,d,*]

[a] Institute of Physical Chemistry, Friedrich Schiller University Jena, Germany
[b] CSIRO Earth Science and Resource Engineering, Kensington, WA, Australia
[c] Geology Department, Faculty of Science, Cairo University, Giza, Egypt
[d] Institute of Photonic Technology, Jena, Germany

HIGHLIGHTS

- The mineralogy of the Upper Cretaceous Duwi phosphorite deposits were investigated.
- Carbonate apatite was the only P-containing mineral detected in the investigated samples.
- Apatite is usually associated with $CaSO_4$ and seldom with $CaCO_3$ in the studied samples.
- Calcium sulfate and goethite are products of diagenesis and weathering.
- The formation of the phosphorite deposits took place in marine environment.

GRAPHICAL ABSTRACT

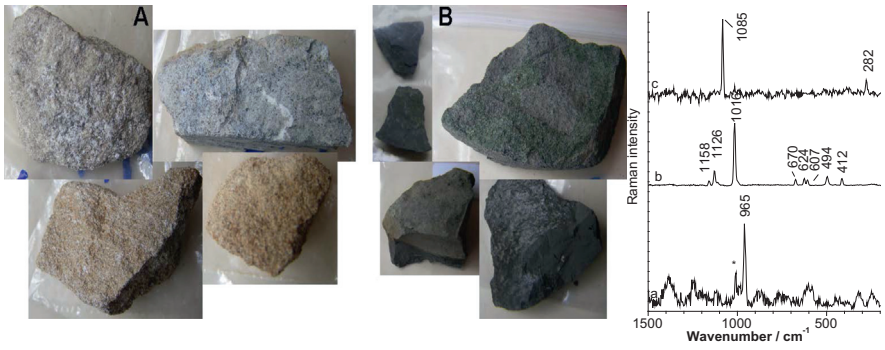

ARTICLE INFO

Article history:
Received 23 May 2013
Received in revised form 6 August 2013
Accepted 14 August 2013
Available online 26 August 2013

Keywords:
Raman spectroscopy
Phosphorite minerals
Apatite

ABSTRACT

The mineral composition of the Upper Cretaceous Duwi phosphorite deposits and underlying Quseir Variegated Shale from Safaga district, Red Sea Range, Egypt, was investigated by dispersive and Fourier transformed Raman spectroscopy. The only phosphorous containing mineral detected in the phosphorite deposits was carbonate fluorapatite. Often carbonate fluorapatite appears associated with calcium sulfate and seldom with calcium carbonate in the investigated samples. Iron is present in the form of goethite and pyrite in the phosphorite layer, while pyrite, marcasite and hematite were identified in the Quseir Shale samples. Also, a high amount of disordered carbon was detected in the black shale layers. The Raman results confirm the hypothesis that the formation of the phosphorites took place in a marine environment. During the formation of black shale, the redox conditions changed, with the pH reaching values of 4 or even lower. Diagenetic and weathering transformations had taken place in the phosphorite deposits, calcium sulfate and goethite being products of these types of processes.

Introduction

Raman spectroscopy became in the last decade a fast and reliable tool in the field of mineral identification [1]. This technique is used for the non-invasive identification of minerals from meteorites [2], characterization of rocks and minerals derived from the Earth's surface [3–6], analysis of atmospheric particles [7,8] or discrimination between similar minerals [9]. In addition, this spectroscopic technique can be used for the detection or identification of organic matter [10,11]. In the art field, Raman spectroscopy is commonly used for the identification of dyes and binding media used by artists [12] or for discrimination between genuine and fake

* Corresponding author at: Institute of Physical Chemistry, Friedrich Schiller University Jena, Germany. Tel.: +49 03641948320.
E-mail address: juergen.popp@uni-jena.de (J. Popp).

1386-1425/$ - see front matter © 2013 Elsevier B.V. All rights reserved.
http://dx.doi.org/10.1016/j.saa.2013.08.059

artifacts [13]. In the last years, this technique has been applied for the investigation of the influence of biotic factors on mineral formation processes [14] and the interaction of microbes with minerals [15]. Therefore, this approach can provide valuable information in the geology/mineralogy field since it can be applied not only for the analysis of abiotic components but also for the study of the interaction between abiotic and biotic components.

The current study is concerned with sedimentary succession in the Wassief area, about 25 km southwest of Port Safaga, Red Sea, between latitudes 26° 25′ and 26° 32′N, and longitudes 33° 48′ and 33° 56′E. The Quseir–Safaga district in the Red Sea land-stretch is covered by Late Cretaceous–Early Tertiary sedimentary sequences [16]. Like most of the Upper Cretaceous–Lower Tertiary sedimentary rocks in the Quseir–Safaga district, the structural pattern of Wassief area is generally a faulted basin [17]. The most characteristic feature in the study area is the dominance of landslides possibly due to capping of highly weathering-liable black shale by hard limestone. The geologic formations of the studied succession are: Quseir, Duwi, Dakhla, Esna, and Thebes formations from base to top. However, the present study focuses on both the Duwi (Phosphorite) and the Quseir (Variegated Shale) formations, since our interest lies on the formation and the diagenesis processes related to the Duwi Formation. The Duwi Formation unconformably overlies the Quseir Variegated Shale and contains the main phosphate beds that belong to the extensive Middle East phosphatic province extending from Syria, Iraq, and Jordan. The province has the greatest accumulation of phosphorites in geological history, the phosphorites being extensively investigated due to their economic importance as fertilizers [18–20]. Phosphorus is the crucial constituent which characterizes the grade of the ore. The P_2O_5 contents range from 14–32% of the Egyptian phosphorites. In the Red Sea and Abu Tartur the calculated P_2O_5 reach 25.81% and 27.95% respectively compared to 27.81% and 28.23% for Nile Valley and 27.48% and 24.94% for Abu Tartur [21].

The origin of the phosphorite and their depositional mechanisms are still subject of some uncertainty [18]. Even the source of phosphorus is controversial; Rittman and Machu believed that ammonium phosphate has been produced by the decay of marine organic matter while Glenn and Arthur suggested that the phosphorus could have originate from a fluvial input [20,22].

More recent studies of the phosphorite deposits seem to agree with the idea that many of the phosphorite deposits appeared as a result of the decomposition of organic matter in marine environments. It is thought that upon progressive burial, the phosphorous weakly bound to organic matter or iron minerals is transformed into autigenic apatite [23].

The aim of the present contribution is to get a better understanding on the formation of the phosphorite deposits and the involved diagenesis processes.

Materials and methods

Samples description

The upper part of the Duwi Formation comprises of black fossiliferous phosphatic limestone, siliceous mottles and micro-veins, as well as disseminated pyrite crystals (Fig. 1A). In Duwi Formation (Fm), there is a band of dark gray fossiliferous dolomite with some pyrite crystals. The phosphatic limestone changes downward into black fossiliferous (forams and pyritized *Pecten* sp.) marl with some phosphatic grains, and disseminated pyrite crystals. Descending, there is about 2.5 m thick band of gray fossiliferous pelletic phosphorite with some pyritization and relative dominance of organic matter. The lowermost part of the Duwi Fm consists of black to light gray massive mudstone with few orange encrusted spots, few calcareous and siliceous micro-veins as well as disseminated pyrite and some phosphatic clastics at the bottom.

The upper part of the Quseir Fm is mainly composed of pyritized glauconitic sandy shale and mudstone of different green, brown and black shades (Fig. 1B). The lower part of the Quseir Formation consists of laminated multicolored mudstone with dispersed pyrite crystals, glauconite and hematitic silty shale. These shales contain limonitic spots as well as some remains of coalified matter. This formation is non-fossiliferous, with the exception of the presence of a few plant remains and fossil wood.

Chemicals and minerals preparation

Calcium nitrate tetrahydrate, $Ca(NO_3)_2{\cdot}4H_2O$ ($\geqslant$99.0%), calcium sulfate dihydrate, $CaSO_4{\cdot}2H_2O$ ($\geqslant$99%), sodium chloride, NaCl (min 99.5%), sodium hydroxide, NaOH ($\geqslant$98%) were purchased from Sigma–Aldrich, while phosphoric acid, H_3PO_4 (85%) and sodium fluoride, NaF (100.0%) were purchased from VWR. These reactants were used without further purification.

Anhydrous $CaSO_4$ (anhydrite) was prepared heating $CaSO_4{\cdot}2H_2O$ at 130 °C for 12 h.

Hydroxyapatite ($Ca_5(PO_4)_3OH$) and fluoroapatite ($Ca_5(PO_4)_3F$) were prepared using the method reported by Sun et al. [24]. Chlorapatite ($Ca_5(PO_4)_3Cl$) was prepared using NaCl instead of NaF in the method to prepare fluoroapatite. For these three cases, the Na_2HPO_4 solution was prepared mixing the appropriate volumes of H_3PO_4 and NaOH solutions, both 0.1 M.

Raman measurements

The dispersive Raman measurements were performed with a commercial micro-Raman setup (HR LabRam inverse system, Jobin Yvon Horiba). A frequency doubled Nd:YAG laser with a wavelength of 532 nm was used as excitation source. To avoid changes in the mineral structure or composition generated by the laser, a power of 40 μW was chosen for the first Raman measurements. The stable minerals were remeasured afterwards using a laser power between 0.4 and 4 mW to obtain better quality Raman spectra. The laser beam was focused on the sample by means of a Zeiss LD EC Epiplan–Neofluar 100 × /0.75 microscope objective down to a spot diameter of approximately 1 μm. The dispersive spectrometer has an entrance slit of 100 μm, a focal length of 800 mm and is equipped with a grating of 300 lines/mm. The Raman scattered light was detected by a Peltier cooled CCD detector. The total acquisition time per spectrum vary between 10 and 150 s.

A Bruker MultiRAM Fourier transform-Raman spectrometer using a 1064 nm Nd:YAG laser and equipped with a cryogenically cooled Ge detector was used for the FT-Raman measurements. The Raman spectra were obtained averaging 500 scans at a 1 cm^{-1} spectral resolution, using 1 W excitation laser power. The apodization was made applying the Blackman–Harris four-term algorithm.

Results and discussion

Mineralogy of phosphorites and black shales

The Raman results presented in this study were obtained using a laser with 532 nm excitation wavelength. Dark color samples are difficult to be analyzed using 1064 nm laser as excitation source, therefore for the characterization of the mineral phases of the both type of samples, phosphorites and black shales, the dispersive Raman configuration has been used.

Apatite (Ca_5 (PO_4, CO_3)$_3$(F, Cl, OH, CO_3)) was the only phosphorus-containing mineral identified in the analyzed phosphorite

Fig. 1. Photographs of the phosphorite deposits (A) and black shales (B).

samples. The main Raman band of apatite is located at ~965 cm^{-1} and is assigned to the symmetric stretching vibration of the P–O bonds (Fig. 2a) [25–27]. As shown in Fig. 2a, the other Raman bands of apatite, which have a much lower intensity, are completely overlapped by the fluorescence background. Anhydrite ($CaSO_4$) was detected in the phosphorite samples, usually associated with apatite. The Raman band marked with an asterisk in Fig. 2a and located at 1016 cm^{-1} belongs to anhydrite [10,28,29]. The strongest Raman band of anhydrous calcium sulfate is assigned to the symmetric stretching vibration of S–O bonds in the SO_4^{2-} tetrahedra. Other Raman bands of the anhydrite mineral are presented at 412, 494, 607, 624, 670, 1126 and 1158 cm^{-1} (Fig. 2b). In addition to apatite and anhydrite, the other calcium-containing mineral detected in the phosphorites was calcite. Small amounts of calcite were identified in the samples based on the characteristic Raman bands at 1085 and 282 cm^{-1} (Fig. 2c) [30–32]. The band at 1085 cm^{-1} is assigned to the symmetric stretching vibration of C–O in CO_3^{2-} ions, while the band at 282 cm^{-1} appears due to external vibrational modes of CO_3^{2-} ions [2]. In the black shales, the only calcium-containing mineral detected was calcite.

Iron-containing minerals are also present in both the phosphorites and the black shales. Goethite (α-FeOOH), the most stable form of iron oxyhydroxide, was detected only in the phosphorites. The most prominent Raman bands of goethite are located at 209, 290, 383 and 680 cm^{-1} (Fig. 3a) [33,34]. However, in black shales hematite (α-Fe_2O_3) was the only form of iron oxide. The Raman spectrum of hematite is shown in Fig. 3b and is dominated by the band at 1320 cm^{-1}. The assignment of this band is still controversial, being assigned to two-magnon scattering or two-phonon scattering of an IR active mode from ~660 cm^{-1} [35,36]. The other Raman bands of hematite occur at 225, 246, 296, 407 and 611 cm^{-1}. Iron sulfides were as well identified in both types of rocks. Pyrite, iron disulfide with a cubic unit cell structure, was detected in phosphorites and black shales. Pyrite presents two strong and sharp Raman bands located at 344 and 377 cm^{-1} (Fig. 3c) [37,38]. Similar to pyrite, the Raman spectrum of marcasite, iron disulfide with an orthogonal unit cell structure, is dominated by two strong Raman bands. However, the Raman bands are shifted to lower and higher wavenumber, respectively, at 323 and 385 cm^{-1} (Fig. 3d) [38,39]. Marcasite was identified only in the black shale probes. In addition to marcasite, the other mineral detected only in black shales was pseudobrookite (Fe_2TiO_5), with the typical Raman bands at 226, 342, 652 and 775 cm^{-1} (Fig. 3e) [40].

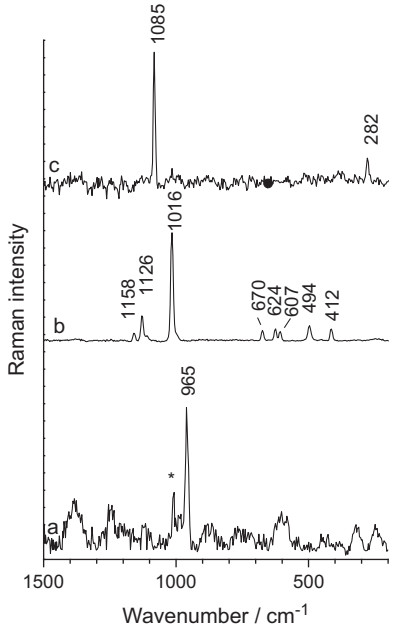

Fig. 2. Raman spectra (532 nm laser excitation) of calcium-containing minerals: (a) apatite, (b) anhydrite, and (c) calcite; (∗) Raman band assigned to anhydrite.

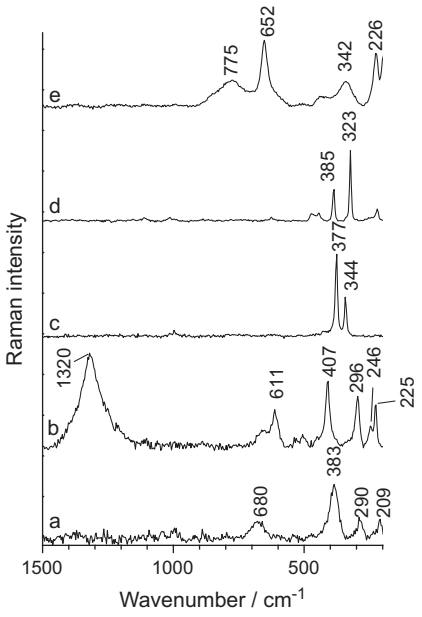

Fig. 3. Raman spectra (532 nm laser excitation) of iron minerals: (a) goethite, (b) hematite, (c) pyrite, (d) marcasite, and (e) pseudobrookite.

Quartz (α-SiO_2) was the only siliceous mineral observed in these two types of rocks considered in this study (Fig. 4a). The strongest Raman bands of quartz occur at 206 and 464 cm^{-1} and are assigned to the symmetry species A1 vibrational modes [41]. In addition to quartz, microcline ($KAlSi_3O_8$) was observed in the black shales (Fig. 4b). The Raman bands assigned to microcline are located at 256, 184, 454, 476 and 513 cm^{-1} [42]. Three characteristic bands at 395, 518 and 638 cm^{-1} can be observed in the Raman spectrum of anatase (TiO_2) (Fig. 4c). Typical for black shales, high amounts of disordered carbon (Fig. 4d) are present in the samples from Quseir Formation.

Investigation of apatite minerals

Apatite minerals can be found in nature as hydroxyapatite, fluorapatite and chlorapatite. In addition, substitutions of cations and anions in apatite occur frequently; particularly important is the case of the carbonate substitution. The carbonate ion can substitute either the PO_4^{2-} tetrahedron or the anion group [25]. Carbonate hydroxyapatite forms the mineral phase of bones and teeth, which, during fossilization alters to a more stable form of apatite, carbonate fluorapatite [43].

The crystal structure of apatite can be described as formed of sixfold Ca columns arranged parallel to the c axis of the crystal, with OH^-, F^- or Cl^- ions located in the void of the columns. The PO_4^{2-} tetrahedra share the space between the Ca columns [44]. The substitution of one anion by another in the crystal structure of apatite can promote some variations in the bond lengths and angles. However, despite the OH^-, F^- and Cl^- ions occupy different positions in the apatite lattice, the effect on the whole apatite structure is minimal, resulting in slight variations on the bond lengths and angles [45] in agreement with the XRD patterns (as shown by Sun et al. [24]). Therefore, the Raman spectra of the three apatite minerals show only minor differences when they are compared to each other (Fig. S1). The Raman signal of symmetric stretching vibration of the PO_4^{2-} groups in hydroxyapatite was reported by Wopenka et al. and Campillo et al. at 962 cm^{-1}, while Penel et al. and Antonakos et al. noticed the Raman band at 963 cm^{-1} [25,44,46,47]. The strongest Raman band in the spectrum of chlorapatite was observed by El Feki et al. and O'Donnell et al. at 961 cm^{-1}, or by Antonakos et al. at 963 cm^{-1} [25,48,49]. In case of fluorapatite, the symmetric stretching vibration of P–O bonds appeared in the Raman spectra recorded by Penel et al. and Campillo et al. at 965 cm^{-1}, while in the Raman spectra acquired by O'Donnell et al. the band has its maximum value at 966 cm^{-1} [44,47,48].

To be able to unambiguously differentiate between the various types of apatite using Raman spectroscopy high spectral resolution measurements are required. Since the values reported in literature for the position of the strongest Raman band of various apatite types differ slightly from one author to the other, various apatite compounds were synthesized in order to create our own Raman databank of apatite spectra. The high spectral resolution measurements were performed with a FT-Raman device and have a resolution of 1 cm^{-1}.

As shown before in Fig. 2a, the strongest band of apatite minerals is the symmetric stretching vibration of the PO_4^{2-} groups appearing in a region around 965 cm^{-1}. The other Raman bands have a much lower intensity and therefore can easily be completely overlapped by the fluorescence background of the sample (see in Fig. 2a) or by the Raman signals of other minerals presented in the investigated spot. This is the reason why in the investigations of heterogeneous samples, very often only the Raman signal of symmetric stretching vibration of the PO_4^{2-} groups is used to distinguish between different types of apatite.

The FT-Raman spectra of synthetic apatites, which are shown in Fig. 5a–c, were used in this study as reference spectra. The Raman band assigned to the symmetric stretching vibration of the PO_4^{2-} groups is centered at 961 cm^{-1} in the spectra of hydroxyapatite and chlorapatite, while in the Raman spectra of fluorapatite the band arise at 964 cm^{-1}. The identity of fluorapatite and hydroxyapatite was confirmed also by the XRD measurements (data not shown). Nevertheless, due to the poor crystallinity of the chlorapatite sample, the mineral could not be unambiguously identified using XRD. Although the positions of Raman bands of the synthesized chlorapatite are in agreement with the previous reports, the possibility that instead of chlorapatite the synthesized mineral is hydroxyapatite cannot be ruled out. However, the presence of chlorapatite in the investigated phosphorite deposits is highly

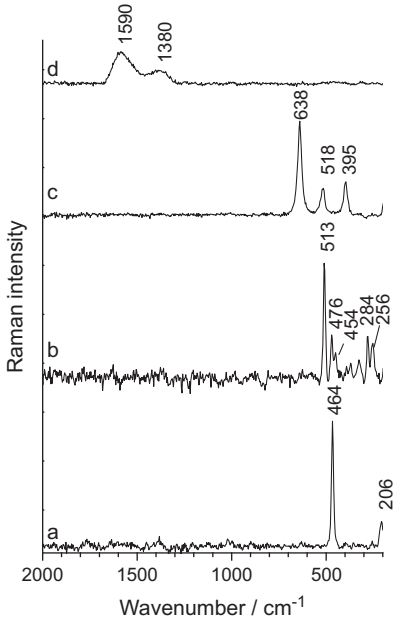

Fig. 4. Raman spectra (532 nm laser excitation) of (a) quartz, (b) microcline, (c) anatase, and (d) disordered carbon.

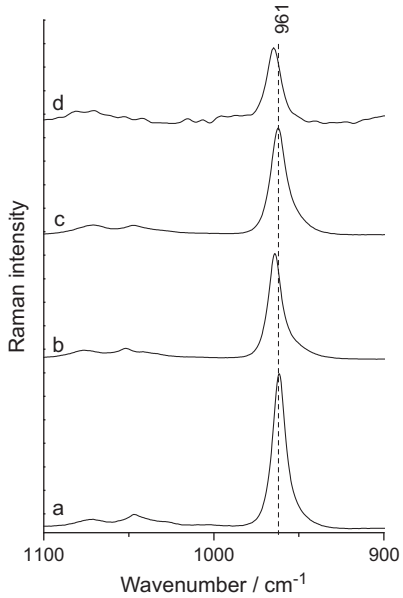

Fig. 5. FT-Raman spectra (1064 nm laser excitation) of (a) hydroxyapatite, (b) fluorapatite, (c) chlorapatite, and (d) phosphorite mineral.

improbable. By using FT-Raman spectroscopy we are able to distinguish between fluorapatite and the other types of apatite.

The phosphorite samples were also analyzed using FT-Raman configuration. In all the FT-Raman spectra of phosphorites containing information from apatite, the symmetric stretching vibration of the PO_4^{2-} groups appears at 965 cm^{-1} (e.g., Fig. 5d). By comparing the acquired phosphorite Raman spectra with the Raman spectra from our database, we can conclude that fluorapatite is the main phosphorus-containing mineral in the phosphorite samples. Raman investigations of the hydroxyapatite fluoridation have shown that a shift of 1 cm^{-1} towards lower wavenumbers in the position of the strongest Raman band of apatite is reached only at a fluoride substitution rate of ca. 90% [44]. Therefore, we can conclude that fluoride represents the major anion species in the measured apatite. The shift of 1 cm^{-1} towards higher wavenumbers of the FT-Raman spectra of phosphorites compared with the Raman spectrum of fluorapatite might be caused by the presence of relatively small amounts of carbonate in the structure of fluorapatite. Small shifts towards higher wavenumbers were observed also by Antonakos et al. in the Raman spectra of natural carbonate fluorapatite [25].

Regarding the origin of the investigated samples, the formation of the phosphorites occurred in a marine environment [18,50]. According to Rittman and Machu, the phosphate minerals were produced from the reaction of calcium carbonate of the associated limestone on sea floor with ammonium phosphate or phosphoric acid produced by the decay of the marine organic matter. The precipitation product is considered to be an amorphous calcium phosphate mineral, which is transformed afterwards into apatite [22]. Skeletal fragments represents a minor component of the phosphorites [20]. The concentration of chloride in the seawater of the modern oceans is circa five orders of magnitude higher than the concentration of fluoride [51]. Keeping in mind that the mineral formation reactions took place in a saline ecosystem having a pH value in the range of 7–8, the precipitation of chlorapatite will be expected if the apatite minerals would have similar solubility. However, the FT-Raman measurements reveal that only carbonate fluorapatite was present in the analyzed samples. The outcome of our study is in agreement with the earlier investigations which reported that fluorapatite rather than chlorapatite or hydroxyapatite is the main type of apatite which occurs in seawater [52,53]. These results can be explained by the tremendous difference in solubility of fluorapatite in comparison with the other types of apatite [54]. The solubility is dependent on the position of the anions in the Ca columns of apatite, the dissolution of the mineral being related to the diffusion capacity of cations in the apatite structure [55]. The diffusion of cations is hindered by the fluorine ions in fluorapatite, diffusion taking place only in the outermost surface layers of the mineral.

Diagenesis and weathering processes

In the Raman investigations performed on phosphorites we identified two different types of iron minerals: pyrite and goethite. In the black shale layer which underlies the phosphorus-containing layer pyrite, marcasite and hematite were detected. Pyrite occurs essentially as framboidal bodies of different sizes. These framboids were formed by microbial activity. The presence of pyrite proposes sedimentation under marine dyoxic conditions. The outcome suggests that changes in the redox conditions took place during the formation of the two deposits, changes which are reflected by the types of iron minerals. The detection of marcasite, an iron sulfide mineral which can be formed only at pH 4 or lower, indicates that acidification of the aquatic environment took place during the black shales formation of the Qusier Formation [56]. This formation which hosts marcasite was deposited under continental conditions before the beginning of the major transgression event that started with the deposition of the Duwi (phosphate) Formation. The variegated shale of the Qusier Formation is rich in allochthonous organic matter derived mostly from terrestrial high plants. The formation of peat and lignin favors formation of marcasite and not pyrite.

The iron oxide and oxyhydroxide from the investigated samples are products of the weathering process. In the phosphorites the ferric ions are stable in the goethite form, while in black shale the iron cations are found in the form of hematite.

In the analyzed samples, apatite minerals ($Ca_5(PO_4, CO_3)_3$(F, Cl, OH, CO_3)) appear often associated with the calcium sulfate minerals and seldom with calcium carbonate. Traditionally, sedimentary apatite is always associated with calcite of both biogenic and chemical origin. Calcium sulfate most probably appears as a result of the oxidation of iron sulfide and the subsequent reaction of sulfuric acid with calcium carbonate.

Conclusions

The outcome of the Raman investigation of phosphorites sustains the theory regarding the formation of the phosphate minerals in a marine environment. The only phosphorus containing mineral detected in the investigated rocks was carbonate fluoroapatite. The transformation of calcium carbonate into calcium sulfate is most probably a result of biotic oxidation of iron sulfide. Changes in the redox conditions during the deposition of phosphorites and black shale are illustrated by the speciation of ferric minerals: pyrite in the phosphorites and marcasite in the black shale layer.

Acknowledgements

We gratefully acknowledge the financial supports from the German Research Foundation (Graduate School 1257 "Alteration and element mobility at the microbe-mineral interface") as well as from the TMBWK (MikroPlex, PE113-1). The authors thank Juraj Majzlan and Ralph Bolanz for the XRD measurements of the synthesized apatite.

Appendix A. Supplementary material

Supplementary data associated with this article can be found, in the online version, at http://dx.doi.org/10.1016/j.saa.2013.08.059.

References

[1] J. Popp, M. Schmitt, Raman spectroscopy breaking terrestrial barriers!, J Raman Spectrosc. 35 (2004) 429–432.
[2] F. Rull Perez, J. Martinez-Frias, Identification of calcite grains in the Vaca Muerta mesosiderite by Raman spectroscopy, J. Raman Spectrosc. 34 (2003) 367–370.
[3] S.K. Sharma, P.G. Lucey, M. Ghosh, H.W. Hubble, K.A. Horton, Stand-off Raman spectroscopic detection of minerals on planetary surfaces, Spectrochim. Acta A 59 (2003) 2391–2407.
[4] S. Cinta Pinzaru, B.P. Onac, Raman study of natural berlinite from a geological phosphate deposit, Vib. Spectrosc. 49 (2009) 97–100.
[5] R.L. Frost, Y. Xi, R. Scholz, F.M. Belotti, A. Lopez, Infrared and Raman spectroscopic characterization of the phosphate mineral fairfieldite – $Ca_2(Mn^{2+}, Fe^{2+})_2(PO_4)_2 \bullet 2(H_2O)$, Spectrochim. Acta A 106 (2013) 216–223.
[6] R.L. Frost, M.L. Weier, K.L. Erickson, O. Carmody, S.J. Mills, Raman spectroscopy of phosphates of the variscite mineral group, J. Raman Spectrosc. 35 (2004) 1047–1055.
[7] H. Rosen, T. Novakov, Raman scattering and the characterisation of atmospheric aerosol particles, Nature 266 (1977) 708–710.
[8] P. Vargas Jentzsch, V. Ciobotă, P. Rösch, J. Popp, Reactions of alkaline minerals in the atmosphere, Angew. Chem. Int. Ed. 125 (2013) 1450–1453.
[9] P. Vargas Jentzsch, R.M. Bolanz, V. Ciobota, B. Kampe, P. Rösch, J. Majzlan, J. Popp, Raman spectroscopic study of calcium mixed salts of atmospheric importance, Vib. Spectrosc. 61 (2012) 206–213.
[10] V. Ciobotă, W. Salama, N. Tarcea, P. Rösch, M.E. Aref, R. Gaupp, J. Popp, Identification of minerals and organic materials in middle eocene ironstones from the bahariya depression in the Western Desert of Egypt by means of micro-Raman spectroscopy, J. Raman Spectrosc. 43 (2012) 405–410.

[11] H.G.M. Edwards, S.E. Jorge Villar, D. Pullan, M.D. Hargreaves, B.A. Hofmann, F. Westall, Morphological biosignatures from relict fossilised sedimentary geological specimens: a Raman spectroscopic study, J. Raman Spectrosc. 38 (2007) 1352–1361.
[12] P. Vandenabeele, B. Wehling, L. Moens, H. Edwards, M. De Reu, G. Van Hooydonk, Analysis with micro-Raman spectroscopy of natural organic binding media and varnishes used in art, Anal. Chim. Acta 407 (2000) 261–274.
[13] H.G.M. Edwards, D.W. Farwell, Ivory and simulated ivory artefacts: Fourier transform Raman diagnostic study, Spectrochim. Acta A 51 (1995) 2073–2081.
[14] M. Reiche, S. Lu, V. Ciobota, T.R. Neu, S. Nietzsche, P. Rösch, J. Popp, K. Küsel, Pelagic boundary conditions affect the biological formation of iron-rich particles (iron snow) and their microbial communities, Limnol. Oceanogr. 56 (2011) 1386–1398.
[15] P. Vítek, H.G.M. Edwards, J. Jehlička, C. Ascaso, A. De Los Ríos, S. Valea, S.E. Jorge-Villar, A.F. Davila, J. Wierzchos, Microbial colonization of halite from the hyper-arid Atacama Desert studied by Raman spectroscopy, Phil. Trans. Roy. Soc. A 368 (2010) 3205–3221.
[16] R. Said, Red Sea Coastal Plain, in: R. Said (Ed.), The Geology of Egypt, Balkema, Rotterdam, Netherlands, 1990, pp. 345–359.
[17] S. Akkad, A. Dardir, Geology and phosphate deposits of Wasif, Safaga area, Egypt. Geolog. Survey 36 (1966) 1–35.
[18] H. Baioumy, R. Tada, Origin of late cretaceous phosphorites in Egypt, Cretaceous Res. 26 (2005) 261–275.
[19] A.M. El-Kammar, E.Z. Basta, Chemical weathering of the economic phosphates of Abu Tartur, Western Desert, Egypt, Chem. Geol. 38 (1983) 321–328.
[20] C.R. Glenn, M.A. Arthur, Anatomy and origin of a cretaceous phosphorite-greensand giant, Egypt, Sedimentology 37 (1990) 123–154.
[21] A. Fakhry, Comparative geochemical studies on phosphorites of North Africa, M.Sc thesis, Cairo University (2009) 109.
[22] N. Rittman, W. Machu, On the origin of Egyptian phosphate deposits, Bull. Faculty Eng. Cairo Univ. 3 (1955) 300–318.
[23] C. März, S.W. Poulton, B. Beckmann, K. Küster, T. Wagner, S. Kasten, Redox sensitivity of P cycling during marine black shale formation: dynamics of sulfidic and anoxic, non-sulfidic bottom waters, Geochim. Cosmochim. Acta 72 (2008) 3703–3717.
[24] B. Sun, H.-Y. Tian, C.-X. Zhang, G. An, Preparation of biomimetic-bone materials and their application to the removal of heavy metals, AIChE J. 59 (2013) 229–240.
[25] A. Antonakos, E. Liarokapis, T. Leventouri, Micro-Raman and FTIR studies of synthetic and natural apatites, Biomaterials 28 (2007) 3043–3054.
[26] E.E. Coleyshaw, W.P. Griffith, R.J. Bowell, Fourier-transform Raman spectroscopy of minerals, Spectrochim. Acta A 50 (1994) 1909–1918.
[27] P. Meuer, A. Wolf, R. Hansch, M. Okrusch, J. Popp, U. Posset, W. Kiefer, FT-Raman-spectroscopic study on the luminescence of synthetic and mineral apatites, Microchim. Acta 133 (2000) 203–207.
[28] P. Makreski, G. Jovanovski, S. Dimitrovska, Minerals from Macedonia: XIV. Identification of some sulfate minerals by vibrational (infrared and Raman) spectroscopy, Vib. Spectrosc. 39 (2005) 229–239.
[29] S.K. Sharma, A.K. Misra, P.G. Lucey, R.C.F. Lentz, A combined remote Raman and LIBS instrument for characterizing minerals with 532 nm laser excitation, Spectrochim. Acta A 73 (2009) 468–476.
[30] H.N. Rutt, J.H. Nicola, Raman spectra of carbonates of calcite structure, J. Phys. C 7 (1974) 4522–4529.
[31] H.G.M. Edwards, D.W. Farwell, M.M. Grady, D.D. Wynn-Williams, I.P. Wright, Comparative Raman microscopy of a Martian meteorite and Antarctic lithic analogues, Planet. Space Sci. 47 (1999) 353–362.
[32] M. Castriota, V. Cosco, T. Barone, G.D. Santo, P. Carafa, E. Cazzanelli, Micro-Raman characterizations of Pompei's mortars, J. Raman Spectrosc. 39 (2008) 295–301.
[33] M.A. Legodi, D. de Waal, The preparation of magnetite, goethite, hematite and maghemite of pigment quality from mill scale iron waste, Dyes Pigments 74 (2007) 161–168.
[34] M. Hanesch, Raman spectroscopy of iron oxides and (oxy)hydroxides at low laser power and possible applications in environmental magnetic studies, Geophys. J. Int. 177 (2009) 941–948.
[35] S.-H. Shim, T.S. Duffy, Raman spectroscopy of Fe_2O_3 to 62 GPa, Am. Mineral. 87 (2002) 318–326.
[36] A. Wang, K.E. Kuebler, B.L. Jolliff, L.A. Haskin, Raman spectroscopy of Fe–Ti–Cr-oxides, case study: Martian meteorite EETA79001, Am. Mineral. 89 (2004) 665–680.
[37] C. Pisapia, B. Humbert, M. Chaussidon, F. Demoisson, C. Mustin, Accurate μ Raman characterization of reaction products at the surface of (bio)oxidized pyrite, Am. Mineral. 95 (2010) 1730–1740.
[38] S.N. White, Laser Raman spectroscopy as a technique for identification of seafloor hydrothermal and cold seep minerals, Chem. Geol. 259 (2009) 240–252.
[39] T. Dörfer, W. Schumacher, N. Tarcea, M. Schmitt, J. Popp, Quantitative mineral analysis using Raman spectroscopy and chemometric techniques, J. Raman Spectrosc. 41 (2010) 684–689.
[40] L.C. Prinsloo, P. Colomban, J.D. Brink, I. Meiklejohn, A Raman spectroscopic study of the igneous rocks on Marion Island: a possible terrestrial analogue for the geology on Mars, J. Raman Spectrosc. 42 (2011) 626–632.
[41] M. Talebian, E. Talebian, A. Abdi, The calculation of active Raman modes of α-quartz crystal via density functional theory based on B3LYP Hamiltonian in 6–311+G(2d) basis set, Pramana – J. Phys. 78 (2012) 803–810.
[42] D.C. Smith, In situ mobile subaquatic archaeometry evaluated by non-destructive Raman microscopy of gemstones lying under impure waters, Spectrochim. Acta A 59 (2003) 2353–2369.
[43] J. Labs-Hochstein, B.J. MacFadden, Quantification of diagenesis in cenozoic sharks: elemental and mineralogical changes, Geochim. Cosmochim. Acta 70 (2006) 4921–4932.
[44] M. Campillo, P.D. Lacharmoise, J.S. Reparaz, A.R. Goni, M. Valiente, On the assessment of hydroxyapatite fluoridation by means of Raman scattering, J. Chem. Phys. 132 (2010) 244501–244505.
[45] J.M. Hughes, M. Cameron, K.D. Crowley, Structural variations in natural F, OH, and Cl apatites, Am. Mineral. 74 (1989) 870–876.
[46] B. Wopenka, J.D. Pasteris, A mineralogical perspective on the apatite in bone, Mat. Sci. Eng. C 25 (2005) 131–143.
[47] G. Penel, G. Leroy, C. Rey, B. Sombret, J.P. Huvenne, E. Bres, Infrared and Raman microspectrometry study of fluor-fluor-hydroxy and hydroxy-apatite powders, J. Mat. Sci. 8 (1997) 271–276.
[48] M.D. O'Donnell, R.G. Hill, R.V. Law, S. Fong, Raman spectroscopy, 19F and 31P MAS-NMR of a series of fluorochloroapatites, J. Europ. Ceram. Soc. 29 (2009) 377–384.
[49] H. El Feki, M. Amami, A. Ben Salah, M. Jemal, Synthesis of potassium chloroapatites, IR, X-ray and Raman studies, Phys. Status Solidi C 1 (2004) 1985–1988.
[50] E.-S. El-Tarabili, Paleogeography, paleoecology and genesis of the phosphatic sediments in the Quseir–Safaga area, U.A.R, Econ. Geol. 64 (1969) 172–182.
[51] T.B. Warner, Normal fluoride content of seawater, Deep Sea Res. 18 (1971) 1255–1263.
[52] J.R. Kramer, Sea water: saturation with apatites and carbonates, Science 146 (1964) 637–638.
[53] E. Atlas, R.M. Pytkowicz, Solubility behaviour of apatites in seawater, Limnol. Oceanogr. 22 (1977) 290–300.
[54] M. Okazaki, H. Tohda, T. Yanagisawa, M. Taira, J. Takahashi, Differences in solubility of two types of heterogeneous fluoridated hydroxyapatites, Biomaterials 19 (1998) 611–616.
[55] R.A. Young, W.V.D. Lugt, J.C. Elliott, Mechanism for fluorine inhibition of diffusion in hydroxyapatite, Nature 223 (1969) 729–730.
[56] J. Schieber, L. Riciputi, Pyrite and marcasite coated grains in the ordovician winnipeg formation, Canada: an intertwined record of surface conditions, stratigraphic condensation, geochemical "reworking", and microbial activity, J. Sediment. Res. 75 (2005) 907–920.